Experimental realization of a dynamic squeezing gate

Kazunori Miyata,[1] Hisashi Ogawa,[1] Petr Marek,[2] Radim Filip,[2] Hidehiro Yonezawa,[3]
Jun-ichi Yoshikawa,[1] and Akira Furusawa[1]

[1]*Department of Applied Physics, School of Engineering, The University of Tokyo, 7-3-1 Hongo, Bunkyo-ku, Tokyo 113-8656, Japan*
[2]*Department of Optics, Palacký University, 17 Listopadu 1192/12, 77146 Olomouc, Czech Republic*
[3]*School of Engineering and Information Technology, University of New South Wales, Canberra, Australian Capital Territory 2600, Australia*

Squeezing is a nonlinear Gaussian operation that is a key component in the construction of other nonlinear
Gaussian gates. In our implementation of the squeezing gate, the amount and the orientation of the squeezing
can be controlled by an external driving signal with a 1-MHz operational bandwidth. This provides another way
to view dynamic Gaussian processing. In particular, the gate can be immediately employed as the feedforward
needed for the deterministic implementation of the quantum cubic phase gate, which is a key piece of universal
quantum information processing.

Quantum information processing with continuous-variable
(CV) systems has many tools. They could be divided
into two broad categories: Gaussian and non-Gaussian. The
Gaussian tools comprise Gaussian quantum states that can
be represented by a Gaussian Wigner function, Gaussian
measurements that project on Gaussian states, and Gaussian operations that transform Gaussian states into different
Gaussian states [1]. The non-Gaussian tools category then
includes everything else. The non-Gaussian category is much
broader and much more powerful. There are many quantum
information protocols that cannot be implemented with Gaussian tools alone; quantum computation [2,3], entanglement
distillation [4–6], and error correction [7] are just the three
most prominent examples.

As a consequence, there is an understandable interest in
all matters non-Gaussian. In quantum optics, which is the
experimental platform of choice when it comes to tests of CV
paradigms [8], the non-Gaussian features need to come from
interactions with discrete-variable physical systems [9–17] or
from discrete measurements [1,7,18,19]. These two general
approaches also differ with respect to quantum systems for
which they can be applied. While the interaction with discrete-variable systems is best realized by a standing-wave mode
in a resonator, the discrete projective measurements work
better with traveling light. There is also another distinction.
The traveling modes of light are much more suitable for
implementation of Gaussian operations. This is significant
because the non-Gaussian resources are useful only when the
Gaussian tools are refined enough to operate without a hitch.
To present a specific example, consider the issue of universal
quantum information processing. In CV systems this means
the ability to implement a unitary operation with an arbitrary
Hamiltonian [2,20]. For this we need to have access to the
cubic operation—a quantum operation with the Hamiltonian
composed of the third power of quadrature operators—*as well
as* the complete range of Gaussian operations.

The Gaussian states, operations, and measurements are the
foundations on which the CV quantum information processing
is built. Homodyne detection, squeezed states, and Gaussian
linear operations in the form of displacement and passive linear
optics are already staples of the contemporary experimental
practice. The measurement-induced paradigm [21], which

employs the passive linear optics together with squeezed states
and linear feedforward, in turn allows implementation of the
Gaussian nonlinear operations such as squeezing [22,23],
quantum nondemolition interaction [24,25], and others
[26–28]. All these past implementations have one thing in
common: The nonlinearity is static. This is not too big of a
problem for the contemporary proof-of-principle experiments
that are built to implement a single specific task. However,
in order to move towards universal and *fast* information
processing, we need operations with a bandwidth higher than
what is allowed by the manual change of optical elements.
The most immediate examples are the proposed experimental
implementation of the cubic phase gate [7,29] and the
experimental preparation of the cubic phase state [7,30], both
of which can be considered to be important first steps towards
universal quantum information processing. These applications
require a nonlinear feedforward, a squeezing operation whose
strength and direction depend on measurement results. In this
Rapid Communication we present the experimental realization
of such an operation for a mode of traveling light. This ensures
that the operation can be used as part of a larger information
processing network, for example, as a feedforward in the
implementation of a cubic phase gate [7,29].

The implemented operation is a time-dependent nonlinear
Gaussian operation with an effective Hamiltonian $\hat{H}(t) = \kappa(t)\hat{x}_{\text{in}}^2(t)$. This operation is in each instant applied to a different
input quantum state $|\psi(t)\rangle_{\text{in}}$. Here $\kappa(t)$ is the strength of
the quadratic operation and $\hat{x}_{\text{in}}(t)$ is the quadrature operator
of $|\psi(t)\rangle_{\text{in}}$. The operation transforms the pair of quadrature
operators as $\hat{x}(t) \rightarrow \hat{x}(t)$ and $\hat{p}(t) \rightarrow \hat{p}(t) + \kappa(t)\hat{x}(t)$, which
can be decomposed into a sequence of a phase shift, a
squeezing, and another phase shift (see Ref. [31]). In this
Rapid Communication we employ a streamlined experimental
configuration that implements the desired transformation up to
a constant local squeezing, which could be effectively compensated by the existing methods [22,23]. The scheme is depicted
in Fig. 1(a) and in the ideal case it works in the following
way: After we combine the input state $|\psi(t)\rangle_{\text{in}}$ with the $\hat{x}$
eigenstate $|x = 0\rangle_S$ at a balanced beam splitter, we measure the
quadrature $\hat{p}_\theta(t) = \hat{p}_{\text{HD}}(t)\cos\theta(t) + \hat{x}_{\text{HD}}(t)\sin\theta(t)$ of one of
the modes by controlling the phase of the local oscillator
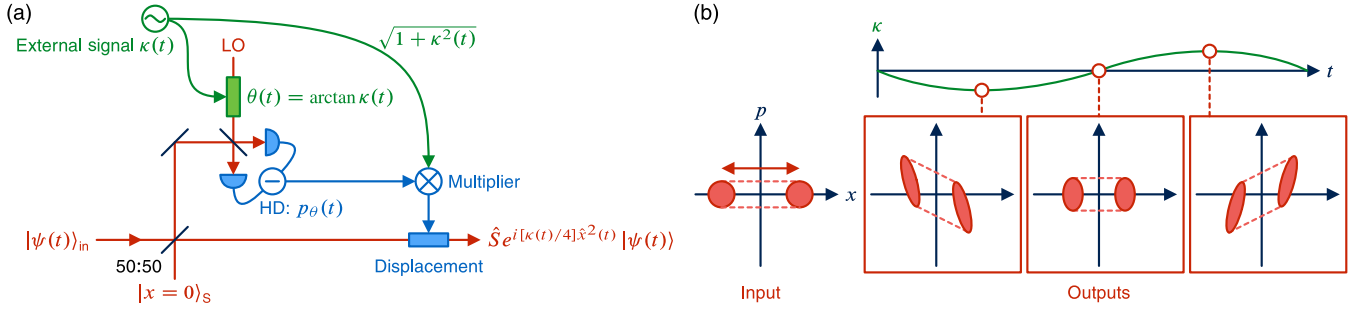(LO) of homodyne detection (HD). Here $\theta(t)$ depends on

FIG. 1. (Color online) (a) Schematic diagram of the dynamic squeezing operation. Here $\hat{S}$ denotes 3-dB squeezing of the $\hat{x}$ quadrature. (b) Illustration of input-output relation of the experiment. Quantum states are depicted as ellipses in the phase-space representation.

the external driving signal as $\theta(t) = \arctan \kappa(t)$. We then use the measured value $p_\theta(t)$ to apply $\hat{p}$ displacement to the unmeasured mode with an electronic gain of $\sqrt{1 + \kappa^2(t)}$. This transforms the quadratures of the output quantum state to $\hat{x}(t) = \hat{x}_{\text{in}}(t)/\sqrt{2}$ and $\hat{p}(t) = \sqrt{2}\hat{p}_{\text{in}}(t) + [\kappa(t)/\sqrt{2}]\hat{x}_{\text{in}}(t)$. With the exception of the constant 3-dB squeezing, which can be efficiently compensated [23], this is exactly the desired form. In reality, we need to approximate the $\hat{x}$ eigenstate $|x = 0\rangle_S$ with a squeezed vacuum state that can be for our purposes completely characterized by its $\hat{x}$-quadrature variance $V_x(t)$. Eventually we can derive the actual input-output relations to be

$$\hat{x}(t) = \frac{1}{\sqrt{2}}\hat{x}_{\text{in}}(t) - \frac{1}{\sqrt{2}}\hat{x}_S(t), \quad (1a)$$

$$\hat{p}(t) = \sqrt{2}\left[\hat{p}_{\text{in}}(t) + \frac{\kappa(t)}{2}\hat{x}_{\text{in}}(t)\right] + \frac{\kappa(t)}{\sqrt{2}}\hat{x}_S(t), \quad (1b)$$

where $\hat{x}_S(t)$ denotes the $\hat{x}$ quadrature of the squeezed vacuum state and vanishes in the limit of infinite squeezing represented by $V_x(t) \to 0$. For the sake of brevity, from now on we will be dropping the explicit notion of time dependence of κ, θ, and other operators.

The input-output relations (1) can be verified by applying the operation to a set of coherent states with differing amplitudes. In our experiment, we have chosen our input to consist of $\hat{x}$-displaced coherent states, whose amplitudes were changed in time. This allowed us to analyze the dynamic behavior with respect to both the gate parameter and the input

state. In practical scenarios we can assume that the control signal is changing more slowly than the input state. If we take one such short interval in which the control signal is constant relative to the fluctuations of the input state, the output state behaves as depicted in Fig. 1(b). When κ is around zero, the signal state is simply squeezed in the x direction and has zero mean amplitude along the p axis. When κ is nonzero in the time interval, the state is displaced in the p direction proportionally to its initial displacement in the x direction and it is also squeezed. The amount and the direction of the squeezing both depend on the value of κ.

The design of our experimental setup is depicted in Fig. 2. The light source is a continuous-wave Ti:sapphire laser operating at 860 nm. The input coherent state is generated at ± 5 MHz around the source-laser frequency with four acousto-optic modulators (AOM). By properly locking relative phases between the frequency-shifted beams, the coherent state is displaced continuously at 5 MHz in the direction of the x axis. (This technique was previously employed in the experiment of Ref. [32].) On the other hand, the ancillary squeezed state is prepared by an optical parametric oscillator (OPO). This OPO is a bow-tie-shaped cavity 300 mm in length, containing a periodically poled KTiOPO$_4$ crystal to obtain second-order nonlinearity. The OPO is pumped by a beam with a wavelength of 430 nm and a power of 120 mW, which is generated by another bow-tie-shaped cavity (second-harmonic generation, SHG) containing a KNbO$_3$ crystal. The bandwidth of the OPO is 12.5 MHz in terms of the half width at half maximum, so our setup sufficiently covers the bandwidth of the input coherent
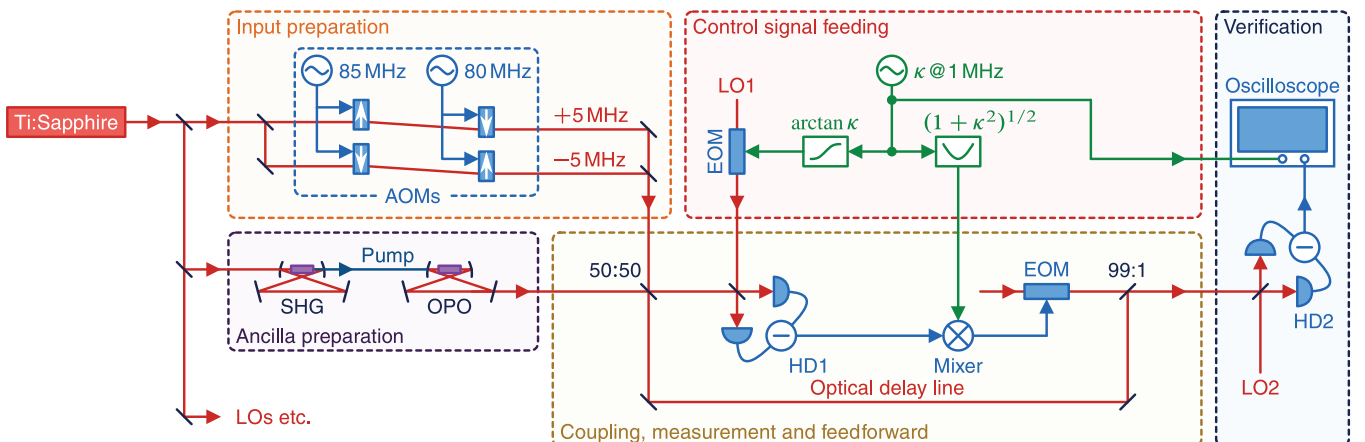

FIG. 2. (Color online) Experimental setup.

state. The typical squeezing level from dc to 10 MHz was −3.1 dB. After the state preparations, we couple the input and the squeezed vacuum at a balanced beam splitter (50:50), measuring one port of the outputs by a homodyne detector (HD1). The measured value is used for the feedforward system, in which the beam of the other port is suitably displaced in the p direction with an electro-optic modulator (EOM), an auxiliary beam, and a slightly transmitting beam splitter (99:1). To match propagation times of the measured signal and the unmeasured optical beam, an optical delay line of 13 m in free space is used. The beam pointing of the delay line is stabilized by a piezoactuated optical mount with a feedback system.

We have a system of feeding a control signal κ, followed by two nonlinear electronic circuits to produce $\arctan \kappa$ and $\sqrt{1 + \kappa^2}$. Here we use a sine wave with a frequency of 1 MHz as the control signal κ. In the measurement process at HD1, the phase θ of the local oscillator (LO1) is controlled by an

EOM to follow the signal $\arctan \kappa$. The measured signal is then amplified by a factor of $\sqrt{1 + \kappa^2}$. For more details on the electronic circuits, which are key components of the dynamic gate, see Ref. [31].

To characterize the output states, we employ another homodyne detector (HD2). Since the initial states are all Gaussian states and the operation is quadratic, the output state is expected to be also Gaussian. Therefore, to characterize the output state by homodyne detection, it is enough to see the mean values and variances of three different bases: the x axis $\hat{x}$, the p axis $\hat{p}$, and the angle of $\pi/4$ from the x axis $\hat{x}_{\pi/4}$. The mean values and variances of the output quadratures are obtained from the measurements repeated 10 851 times. The control signal κ for each measurement is collected together.

Figure 3 shows the experimental mean values and variances (normalized as $\hbar = 1$). All the results are plotted in the same time domain. Figure 3(a) represents the supplied control signal
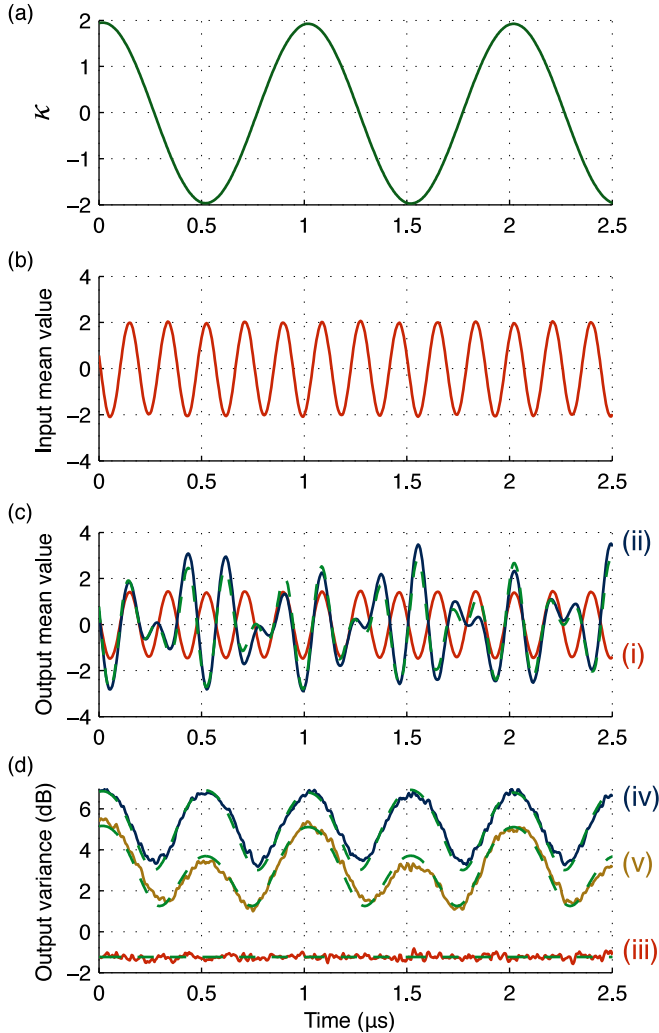

FIG. 3. (Color online) Experimental mean values and variances compared with theoretical predictions ($\hbar = 1$). (a) Supplied control signal. (b) Mean $\hat{x}$-quadrature values $\langle \hat{x}_{\rm in} \rangle$ of the input coherent states. Mean $\hat{p}$-quadrature values are omitted because they are always zero. (c) Mean quadrature values of the output: (i) $\langle \hat{x} \rangle$ and (ii) $\langle \hat{p} \rangle$. (d) Variances of the output quadratures relative to that of the shot noise: (iii) $\langle \Delta \hat{x}^2 \rangle$, (iv) $\langle \Delta \hat{p}^2 \rangle$, and (v) $\langle \Delta \hat{x}_{\pi/4}^2 \rangle$. Solid curves are experimental results, while dashed curves are theoretical predictions.
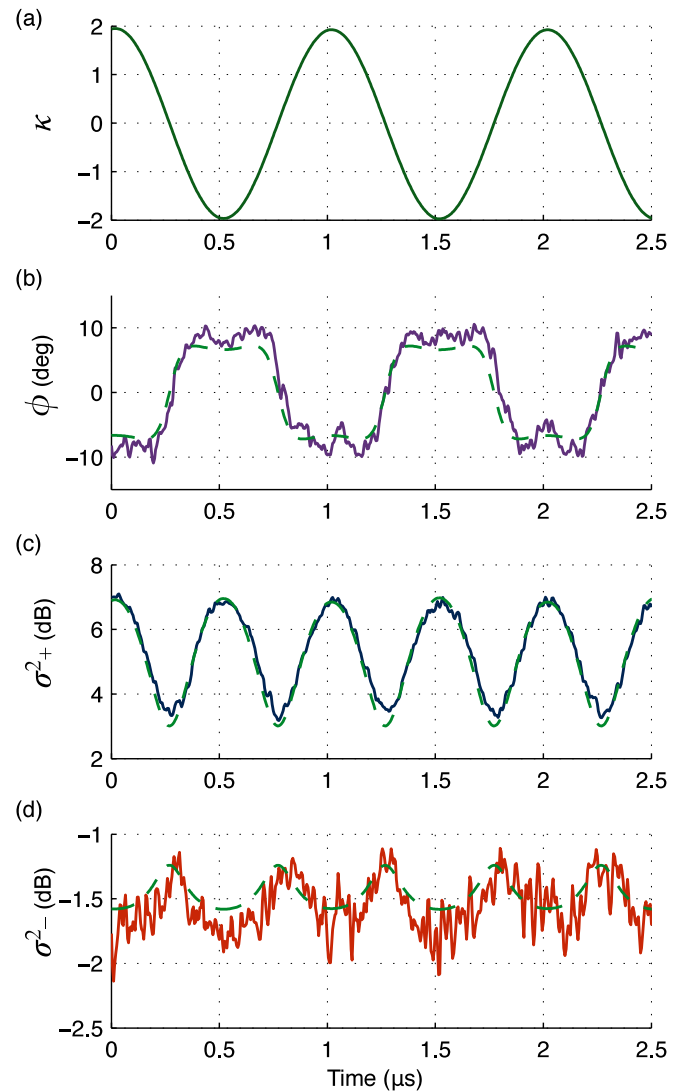

FIG. 4. (Color online) Analysis of the output states in terms of their diagonalized variance matrices. (a) Supplied control signal. (b) Squeezing angles of the output states. (c) Maximally antisqueezed variances and (d) maximally squeezed variances relative to the shot-noise variance. Solid curves are experimental results calculated from those in Fig. 3, while dashed curves are theoretical predictions.

κ at 1 MHz. Figure 3(b) shows the mean $\hat{x}$-quadrature values $\langle\hat{x}_{\rm in}\rangle$ of the input states, continuously fluctuating at 5 MHz. The values in Fig. 3(b) were measured after the balanced beam splitter, whose attenuation is compensated numerically by multiplying by $\sqrt{2}$. The mean values of the p quadrature are confirmed to be zero before the measurement. Figure 3(c) shows the mean values $\langle\hat{x}\rangle$ and $\langle\hat{p}\rangle$ of the output states. From Eq. (1), $\langle\hat{x}\rangle$ should be independent of κ, while $\langle\hat{p}\rangle$ is proportional to $\kappa\langle\hat{x}_{\rm in}\rangle$. As expected, the oscillation of $\langle\hat{p}\rangle$ behaves in phase or out of phase with the oscillation of $\langle\hat{x}\rangle$ in accordance with whether κ is positive or negative and vanishes when κ is zero. Similarly, as seen in Fig. 3(d), the variances of the $\hat{x}$ quadrature are constantly squeezed by -1.3 dB, while the variances of the $\hat{p}$ quadrature oscillate at twice the frequency of the control signal κ in accord with the relation $\langle\Delta\hat{p}^2\rangle = 2\langle\Delta\hat{p}_{\rm in}^2\rangle + (\kappa^2/2)\langle\Delta\hat{x}_{\rm in}^2\rangle$. Including the variances of $\hat{x}_{\pi/4}$ quadrature, those characteristics agree well with theoretical predictions plotted with dashed curves.

We have also analyzed the output states in terms of their squeezing in both magnitude and direction. For each individual time window we have reconstructed the variance matrices of the output states as

$$V = \begin{pmatrix} \sigma_x^2 & \sigma_{xp} \\ \sigma_{xp} & \sigma_p^2 \end{pmatrix}, \tag{2a}$$

$$\sigma_{xp} = \frac{1}{2}\langle\hat{x}\hat{p} + \hat{p}\hat{x}\rangle = \sigma_{\pi/4}^2 - \frac{1}{2}\left(\sigma_x^2 + \sigma_p^2\right), \tag{2b}$$

where $\sigma_x^2 = \langle\Delta\hat{x}^2\rangle$, $\sigma_p^2 = \langle\Delta\hat{p}^2\rangle$, and $\sigma_{\pi/4}^2 = \langle\Delta\hat{x}_{\pi/4}^2\rangle$ are the variances directly obtained from the measured data. The variances of the squeezed and the antisqueezed quadratures, which are denoted by σ_-^2 and σ_+^2, respectively, are then found as the eigenvalues of the variance matrix (2a),

$$\sigma_+^2 = \sigma_x^2\sin^2\phi + \sigma_p^2\cos^2\phi + 2\sigma_{xp}\sin\phi\cos\phi, \tag{3a}$$

$$\sigma_-^2 = \sigma_x^2\cos^2\phi + \sigma_p^2\sin^2\phi - 2\sigma_{xp}\sin\phi\cos\phi, \tag{3b}$$

$$\phi = \frac{1}{2}\arctan\left(\frac{-2\sigma_{xp}}{\sigma_x^2 - \sigma_p^2}\right). \tag{3c}$$

Here the parameter ϕ determines the direction of the squeezing, with $\phi = 0$ describing the situation in which $\hat{x}$ quadrature is squeezed. We have compared the values (3) obtained from the experimental data with the theoretical predictions and the results can be seen in Fig. 4. Figure 4(a) represents again the supplied control signal κ. Figure 4(b) shows the angles of the squeezing axes ϕ. The square-wave-like behavior of the resulting angles means that the output states are properly rotated in phase space. Figures 4(c) and 4(d) show the maximally antisqueezed variances σ_+^2 and the maximally squeezed variances σ_-^2, respectively. The maximal antisqueezing starts from about 3 dB where the control signal vanishes and reaches about 7 dB with $\kappa = \pm2$. For the maximal squeezing, it starts from about -1.3 dB and reaches about -1.8 dB. While these values are reduced from those of the ideal case due to the finite squeezing of the ancillary states, they still show a dependence on the control signal and agree well with theoretical predictions (dashed curves).

In conclusion, we have experimentally demonstrated a squeezing operation whose squeezing level and squeezing direction can be continuously adjusted with an operational bandwidth of 1 MHz. This dynamic squeezing gate can allow implementation of an arbitrary dynamic Gaussian gate [33] and significantly expands the possibilities of teleportation-based quantum operations. On a more immediate time scale, the squeezing gate is now ready to serve as the feedforward part of the cubic phase gate [7,29]. Since the cubic phase state has already been experimentally realized [19], the full implementation of the cubic phase gate required for the universal CV quantum information processing can be expected.

[1] A. Furusawa and P. van Loock, *Quantum Teleportation and Entanglement: A Hybrid Approach to Optical Quantum Information Processing* (Wiley, Weinheim, 2011).

[2] S. Lloyd and S. L. Braunstein, Phys. Rev. Lett. **82**, 1784 (1999).

[3] N. C. Menicucci, P. van Loock, M. Gu, C. Weedbrook, T. C. Ralph, and M. A. Nielsen, Phys. Rev. Lett. **97**, 110501 (2006).

[4] J. Fiurášek, Phys. Rev. Lett. **89**, 137904 (2002).

[5] G. Giedke and J. I. Cirac, Phys. Rev. A **66**, 032316 (2002).

[6] J. Eisert and M. B. Plenio, Int. J. Quantum Inf. **01**, 479 (2003).

[7] D. Gottesman, A. Kitaev, and J. Preskill, Phys. Rev. A **64**, 012310 (2001).

[8] S. L. Braunstein and P. van Loock, Rev. Mod. Phys. **77**, 513 (2005).

[9] S. Deléglise, I. Dotsenko, C. Sayrin, J. Bernu, M. Brune, J.-M. Raimond, and S. Haroche, Nature (London) **455**, 510 (2008).

[10] H.-Y. Lo, P.-C. Su, and Y.-F. Chen, Phys. Rev. A **81**, 053829 (2010).

[11] T. Peyronel, O. Firstenberg, Q.-Y. Liang, S. Hofferberth, A. V. Gorshkov, T. Pohl, M. D. Lukin, and V. Vuletić, Nature (London) **488**, 57 (2012).

[12] C. Sames, H. Chibani, C. Hamsen, P. A. Altin, T. Wilk, and G. Rempe, Phys. Rev. Lett. **112**, 043601 (2014).

[13] T. G. Tiecke, J. D. Thompson, N. P. de Leon, L. R. Liu, V. Vuletić, and M. D. Lukin, Nature (London) **508**, 241 (2014).

[14] D. Leibfried, R. Blatt, C. Monroe, and D. Wineland, Rev. Mod. Phys. **75**, 281 (2003).

[15] A. Wallraff, D. I. Schuster, A. Blais, L. Frunzio, R.-S. Huang, J. Majer, S. Kumar, S. M. Girvin, and R. J. Schoelkopf, Nature (London) **431**, 162 (2004).

[16] M. Hofheinz, H. Wang, M. Ansmann, R. C. Bialczak, E. Lucero, M. Neeley, A. D. O'Connell, D. Sank, J. Wenner, J. M. Martinis, and A. N. Cleland, Nature (London) **459**, 546 (2009).

[17] G. Kirchmair, B. Vlastakis, Z. Leghtas, S. E. Nigg, H. Paik, E. Ginossar, M. Mirrahimi, L. Frunzio, S. M. Girvin, and R. J. Schoelkopf, Nature (London) **495**, 205 (2013).

[18] M. Yukawa, K. Miyata, T. Mizuta, H. Yonezawa, P. Marek, R. Filip, and A. Furusawa, Opt. Express **21**, 5529 (2013).

[19] M. Yukawa, K. Miyata, H. Yonezawa, P. Marek, R. Filip, and A. Furusawa, Phys. Rev. A **88**, 053816 (2013).

[20] S. D. Bartlett and B. C. Sanders, Phys. Rev. A **65**, 042304 (2002).

[21] R. Filip, P. Marek, and U. L. Andersen, Phys. Rev. A **71**, 042308 (2005).

[22] J. Yoshikawa, T. Hayashi, T. Akiyama, N. Takei, A. Huck, U. L. Andersen, and A. Furusawa, Phys. Rev. A **76**, 060301(R) (2007).

[23] Y. Miwa, J. Yoshikawa, N. Iwata, M. Endo, P. Marek, R. Filip, P. van Loock, and A. Furusawa, Phys. Rev. Lett. **113**, 013601 (2014).

[24] J. Yoshikawa, Y. Miwa, A. Huck, U. L. Andersen, P. van Loock, and A. Furusawa, Phys. Rev. Lett. **101**, 250501 (2008).

[25] S. Yokoyama, R. Ukai, J. Yoshikawa, P. Marek, R. Filip, and A. Furusawa, Phys. Rev. A **90**, 012311 (2014).

[26] J. Yoshikawa, Y. Miwa, R. Filip, and A. Furusawa, Phys. Rev. A **83**, 052307 (2011).

[27] Y. Miwa, J. Yoshikawa, P. van Loock, and A. Furusawa, Phys. Rev. A **80**, 050303(R) (2009).

[28] R. Ukai, N. Iwata, Y. Shimokawa, S. C. Armstrong, A. Politi, J. Yoshikawa, P. van Loock, and A. Furusawa, Phys. Rev. Lett. **106**, 240504 (2011).

[29] P. Marek, R. Filip, and A. Furusawa, Phys. Rev. A **84**, 053802 (2011).

[30] M. Gu, C. Weedbrook, N. C. Menicucci, T. C. Ralph, and P. van Loock, Phys. Rev. A **79**, 062318 (2009).

[31] See Supplemental Material at http://link.aps.org/supplemental/10.1103/PhysRevA.90.060302 for information on nonlinear electric circuits and also on decomposition of the quadratic gate.

[32] H. Yonezawa, D. Nakane, T. A. Wheatley, K. Iwasawa, S. Takeda, H. Arao, K. Ohki, K. Tsumura, D. W. Berry, T. C. Ralph, H. M. Wiseman, E. H. Huntington, and A. Furusawa, Science **337**, 1514 (2012).

[33] S. L. Braunstein, Phys. Rev. A **71**, 055801 (2005).